Translational Oncology
www.transonc.com
Volume 9 Number 1 February 2016 pp. 8–17 8

Early Prediction and Evaluation of Breast Cancer Response to Neoadjuvant Chemotherapy Using Quantitative DCE-MRI[1]

Alina Tudorica*, Karen Y Oh*, Stephen Y-C Chui†,‡, Nicole Roy*, Megan L Troxell‡,§, Arpana Naik‡,¶, Kathleen A Kemmer†,‡, Yiyi Chen‡,#, Megan L Holtorf‡, Aneela Afzal, Charles S Springer Jr. ‡,**, Xin Li** and Wei Huang‡,****

*Diagnostic Radiology, Oregon Health & Science University, Portland, OR, USA; †Medical Oncology, Oregon Health & Science University, Portland, OR, USA; ‡Knight Cancer Institute, Oregon Health & Science University, Portland, OR, USA; §Pathology, Oregon Health & Science University, Portland, OR, USA; ¶Surgical Oncology, Oregon Health & Science University, Portland, OR, USA; #Public Health and Preventive Medicine, Oregon Health & Science University, Portland, OR, USA; **Advanced Imaging Research Center, Oregon Health & Science University, Portland, OR, USA

Abstract

The purpose is to compare quantitative dynamic contrast-enhanced (DCE) magnetic resonance imaging (MRI) metrics with imaging tumor size for early prediction of breast cancer response to neoadjuvant chemotherapy (NACT) and evaluation of residual cancer burden (RCB). Twenty-eight patients with 29 primary breast tumors underwent DCE-MRI exams before, after one cycle of, at midpoint of, and after NACT. MRI tumor size in the longest diameter (LD) was measured according to the RECIST (Response Evaluation Criteria In Solid Tumors) guidelines. Pharmacokinetic analyses of DCE-MRI data were performed with the standard Tofts and Shutter-Speed models (TM and SSM). After one NACT cycle the percent changes of DCE-MRI parameters K^{trans} (contrast agent plasma/interstitium transfer rate constant), v_e (extravascular and extracellular volume fraction), k_{ep} (intravasation rate constant), and SSM-unique τ_i (mean intracellular water lifetime) are good to excellent early predictors of pathologic complete response (pCR) *vs.* non-pCR, with univariate logistic regression C statistics value in the range of 0.804 to 0.967. v_e values after one cycle and at NACT midpoint are also good predictors of response, with C ranging 0.845 to 0.897. However, RECIST LD changes are poor predictors with C = 0.609 and 0.673, respectively. Post-NACT K^{trans}, τ_i, and RECIST LD show statistically significant ($P < .05$) correlations with RCB. The performances of TM and SSM analyses for early prediction of response and RCB evaluation are comparable. In conclusion, quantitative DCE-MRI parameters are superior to imaging tumor size for early prediction of therapy response. Both TM and SSM analyses are effective for therapy response evaluation. However, the τ_i parameter derived only with SSM analysis allows the unique opportunity to potentially quantify therapy-induced changes in tumor energetic metabolism.

Translational Oncology (2016) 9, 8–17

Introduction

Neoadjuvant chemotherapy (NACT) is commonly used as standard of care treatment for locally advanced breast cancer with the primary clinical goals of downstaging the disease, improving operability, and allowing breast conserving surgery [1,2]. Though NACT does not improve overall survival in comparison with postoperative adjuvant therapy [3–5], one advantage of NACT is to provide the opportunity for assessment of pathologic response to the treatment. Pathologic

Address all correspondence to: Wei Huang, PhD, Advanced Imaging Research Center, Oregon Health & Science University, 3181 SW Sam Jackson Park Road, Portland, OR 97239.
E-mail: huangwe@ohsu.edu

[1] Financial Support: This study was supported by NIH grants U01-CA154602 and R44-CA180425.
Received 7 September 2015; Revised 20 November 2015; Accepted 23 November 2015

1936-5233/16
http://dx.doi.org/10.1016/j.tranon.2015.11.016

complete response (pCR) or minimal residual disease following NACT has been shown to be prognostic for survival [6–9]. The majority of the patients, however, do not achieve pCR with the pCR rate reported in the range of 6% to 45% depending on breast cancer subtypes and treatment regimens [6,7,10,11]. Furthermore, the pathologic response status is generally determined only from the surgical specimen after NACT completion. Therefore, there is a genuine and unmet need for reliable and minimally invasive imaging methods to provide early prediction of response to NACT. In the emerging era of precision medicine, early prediction of NACT response may allow rapid, personalized treatment regimen alterations for non-responding breast cancer patients and spare them from potential short and long term toxicities associated with ineffective therapies. Additionally, accurate evaluation of residual disease after NACT is vital for surgical decision making and could result in surgical treatment plans more tailored to individual patients.

Imaging tumor size change with guidelines such as RECIST (Response Evaluation Criteria In Solid Tumors) [12] is routinely used in clinical trial settings to assess tumor response to treatment. However, size change in response to therapy is often found to manifest later than changes in underlying tumor functions [13–16], such as vascularization and vascular permeability, cellularity, and metabolism. Recognized as a minimally invasive imaging method for evaluation of perfusion and permeability, dynamic contrast-enhanced magnetic resonance imaging (DCE-MRI) is increasingly used in research and early phase clinical trial settings to measure and, importantly, predict tumor response to treatment [13,14]. Over the last decade, substantial evidence has accumulated [17–19] showing the utility of DCE-MRI for assessment and early prediction of breast cancer response to NACT. Despite large variations in DCE-MRI data acquisition protocol details (temporal resolution, spatial resolution and coverage, acquisition time length, etc.) and data analysis methods (semi-quantitative *vs.* quantitative pharmacokinetic analysis of signal intensity time-course data), many studies have shown that changes in several semi-quantitative [20–25] or quantitative [26–35] DCE-MRI metrics during the course of NACT can provide good early prediction of pathologic response after one to two NACT cycles, and valuable clinical evaluation of overall response and prognosis. In correlating DCE-MRI parameters with pathologic response endpoints, most studies use binary discrimination of pCR and non-pCR with few [23] reporting relationships between post-NACT imaging metrics and pathologically measured residual disease burden, which could have important implications for surgical decision making. Among studies that performed quantitative pharmacokinetic analyses of DCE-MRI data, most employed the nuclear medicine, tracer kinetic model based Tofts model (TM) [36,37] with inherent neglect of the effects of intercompartmental water exchange kinetics. The water molecule is not the signal molecule in nuclear medicine imaging, but in DCE-MRI it is. Considering the two-compartment model of intra- and extra-cellular spaces, for example, since contrast agent (CA) molecules generally reside in the extracellular space, the cross-cell membrane water exchange kinetics needs to be accounted for when converting MRI signal intensity change to tissue CA concentration change in pharmacokinetic analysis of DCE-MRI data.

In this paper we report our initial results in DCE-MRI assessment of breast cancer response to NACT. The DCE-MRI data were analyzed using both the TM and the Shutter-Speed model (SSM), which takes into account the finite intercompartmental water exchange kinetics [38,39]. DCE-MRI parameters, including the SSM-unique τ_i parameter (mean intracellular water lifetime), an inverse measure of cellular metabolic activity [40,41], were evaluated and compared between the TM and SSM and with imaging tumor size measurement, for early prediction of pathologic response to NACT and assessment of residual disease.

Materials and Methods

Patient Cohort and Study Schema

In this institutional review board–approved and HIPAA-compliant study, twenty-eight women who were diagnosed with 29 grade 2 to 3 invasive breast tumors (one patient had two independent primary tumors) and to undergo NACT were consented to participate in a longitudinal research MRI study that includes DCE-MRI. Twenty one (22 primary tumors) of the 28 patients were treated with standard of care therapy regimens that include four cycles of doxorubicin-cyclophosphamide every 2 weeks followed by four cycles of a taxane every 2 weeks, or six cycles of the combination of all three drugs every 3 weeks. The targeted agent, trastuzumab, was added to the regimen for tumors with positive HER2 (human epidermal growth factor receptor 2) receptor status. The other seven patients (seven primary tumors) were enrolled in the NACT ISPY-2 trial (http://ispy2.org), where patients were randomized to receive standard of care regimen or standard of care regimen plus experimental drugs. The ISPY-2 standard of care regimen starts with a taxane, followed by doxorubicin-cyclophosphamide. If used, the experimental drug is usually added to the taxane. Four of the seven patients were placed in the treatment arm with experimental drugs: three (patient 7, 12, and 13, Table 1) received neratinib, a tyrosine kinase inhibitor, and the other (patient 24) received ganitumab, a human monoclonal antibody against type 1 insulin-like growth factor receptor (IGF1R). The clinicopathologic characteristics of the studied patient cohort are presented in Table 1.

The MRI exams for this research study were performed pre-NACT (Visit 1, V1), after one cycle of NACT (V2), at midpoint of NACT (V3; usually after 3 or 4 cycles of NACT, or before change of NACT agents), and after NACT completion but prior to surgery (V4). The ISPY-2 trial includes a different MRI protocol conducted at the same four time points. For the 7 patients who participated in the ISPY-2 trial, care was taken to ensure there were at least 24 hours between the research and ISPY-2 MRI studies to allow CA, used in both, clearance from the body. For the V2 – V4 studies, the MRI scan was undertaken at least 7 days after the administration of the previous NACT cycle to allow time for drug effects.

DCE-MRI Data Acquisition

All breast MRI studies were performed using a 3 T Siemens Tim Trio system with the body coil and a four-channel bilateral phased-array breast coil as the transmitter and receiver, respectively. In each MRI session, following pilot scans and pre-CA axial T_2-weighted MRI with fat-saturation and axial T_1-weighted MRI without fat-saturation, axial bilateral DCE-MRI images with fat-saturation (using the approach of water excitation only) and full breast coverage were acquired with a 3D gradient echo-based TWIST (Time-resolved angiography WIth Stochastic Trajectories) sequence, which employs the strategy of k-space undersampling during acquisition and data sharing during reconstruction [42]. Compared to conventional full k-space sampling gradient echo sequences, the TWIST sequence enables acceleration of image acquisition and preserves signal-to-noise ratio, while the image artifacts can be minimized using appropriate k-space undersampling and view sharing

Table 1. Clinicopathologic Characteristics of the Study Patient Cohort Treated with Neoadjuvant Chemotherapy

Patient Number	Age (yr)	Tumor Type	Tumor Grade	Pre-treatment Size (cm)	Receptor Status(ER,PR,HER2)	Treatment Regimen	Pathologic Response	RCB Class
1	27	IDC	2	3.7(Mammo)	–, –, +	Docetaxel + carboplatin + trastuzumab	non-pCR	III
2	27	IDC	2	1.3(MRI)	+, +, +	Docetaxel + carboplatin + trastuzumab	pCR	0
3	61	IDC	3	2.4(MRI)	–, –, –	Adriamycin + cyclophosphamide, then paclitaxel	non-pCR	I
4	39	IDC	2	2.6(MRI)	+, +, +	Paclitaxel + trastuzumab, then cyclophosphamide + adriamycin	pCR	0
5	63	IDC	2	2.3(US)	–, –, +	Docetaxel + carboplatin + trastuzumab	pCR	0
6	56	IDC	3	4.4(US)	–, –, –	Paclitaxel, then cyclophosphamide + adriamycin	non-pCR	I
7	62	IDC	3	2.1(Mammo)	–, –, –	Carboplatin + neratinib, then cyclophosphamide + adriamycin	non-pCR	II
8	65	IDC	2	2.1(Mammo)	+, +, –	Cyclophosphamide + adriamycin, then paclitaxel	non-pCR	II
9	46	IDC	2	2.5(Mammo)	+, +, –	Cyclophosphamide + adriamycin + docetaxel	non-pCR	II
10	33	IDC	2	2.0(US)	+, +, +	Docetaxel + carboplatin + trastuzumab	non-pCR	II
11	41	IDC	2	3.0(MRI)	+, +, -	Cyclophosphamide + adriamycin + docetaxel	non-pCR	II
12	35	IDC	2	2.8(MRI)	–, +, +	Paclitaxel + neratinib, then cyclophosphamide + adriamycin	pCR	0
13	39	IDC	3	2.7(MRI)	+, –, +	Paclitaxel + neratinib, then cyclophosphamide + adriamycin	non-pCR	I
14	42	IDC	2	1.6(US)	+, +, +	Doxorubicin + cyclophosphamide, then docetaxel + trastuzumab	non-pCR	II
		IDC	2	1.8(US)	+, –, –		non-pCR	I
15	34	IDC	2	5.0(MRI)	+, +, –	Paclitaxel, then cyclophosphamide + adriamycin	non-pCR	II
16	45	ILC	2	11.8(MRI)	+, +, –	Paclitaxel, then cyclophosphamide + adriamycin	non-pCR	III
17	38	IDC	3	3.6(US)	–, –, +	Docetaxel + carboplatin + trastuzumab	non-pCR	III
18	59	IDC	3	2.0(US)	+, +, +	Docetaxel + carboplatin + trastuzumab	non-pCR	II
19	46	IDC	3	1.7(US)	–, –, +	Docetaxel + carboplatin + trastuzumab	non-pCR	I
20	59	IDC	2	3.0(MRI)	–, –, +	Paclitaxel + trastuzumab, then cyclophosphamide + adriamycin	pCR	0
21	51	IDC	2	3.2(Mammo)	+, +, –	Cyclophosphamide + Adriamycin + docetaxel	non-pCR	I
22	75	ILC	2	2.5(Mammo)	–, –, –	Adriamycin + cyclophosphamide, then paclitaxel	non-pCR	II
23	34	IDC	3	2.1(MRI)	–, –, +	Adriamycin + cyclophosphamide, then paclitaxel + trastuzumab	non-pCR	I
24	32	IDC	3	5.9(MRI)	+, +, –	Paclitaxel + ganitumab, then cyclophosphamide + adriamycin	non-pCR	II
25	44	IDC	2	2.8(MRI)	+, +, –	Adriamycin + cyclophosphamide, then paclitaxel	non-pCR	I
26	37	IDC	3	9.8(MRI)	–, –, –	Cyclophosphamide + Adriamycin + docetaxel	non-pCR	II
27	48	IDC	3	2.9(Mammo)	–, +, –	Adriamycin + cyclophosphamide, then paclitaxel	non-pCR	III
28	31	IDC	3	1.6(US)	–, +, –	Adriamycin + cyclophosphamide, then paclitaxel	non-pCR	I

IDC: invasive ductal carcinoma; ILC: invasive lobular carcinoma; Pre-treatment size: imaging tumor size in the longest diameter before treatment; Mammo: mammography; US: ultrasound; ER: estrogen receptor; PR: progesterone receptor; HER2: human epidermal growth factor receptor 2; pCR: pathologic complete response; RCB: residual cancer burden.

strategies [42]. DCE-MRI acquisition parameters included 10° flip angle, 2.9/6.2 ms TE/TR, a parallel imaging acceleration factor of 2, 30 to 34 cm FOV, 320×320 in-plane matrix size, and 1.4 mm slice thickness. The total acquisition time for a DCE-MRI series was ~10 minutes for 28 to 38 image volume sets of 96 to 128 slices each with 14.6 to 20.2 s temporal resolution. The variations in number of image volumes, number of slices per volume, and temporal resolution were due to differences in breast size. The intravenous injection of the CA, Gd(HP-DO3A) [ProHance (Bracco Diagnostic Inc.)] (0.1 mmol/kg at 2 mL/s), by a programmable power injector was timed to commence after acquisition of two baseline image volumes, followed by a 20-mL saline flush.

For quantification of the pre-CA T_1 value, T_{10}, proton density-weighted images were acquired immediately before and spatially co-registered with the DCE-MRI scan [42,43]. The data acquisition sequence and parameters were the same as for the DCE-MRI scan except for 5° flip angle and 50 ms TR.

DCE-MRI Data Analysis

Breast tumor regions of interest (ROIs) were drawn by two experienced breast radiologists on post-CA (approximately 90 to 120 s after the CA injection) multi-slice DCE images covering the entire contrast-enhanced tumor. They also measured the longest diameter (LD) of the tumor from these images using the RECIST guidelines [12]. To avoid within-subject inter-observer variations, all images from the longitudinal study of a given patient were interpreted by one radiologist.

For the purpose of pharmacokinetic modeling of DCE-MRI data, the tumor ROI- and voxel-based T_{10} value was determined by comparing signal intensities between the proton density-weighted images and the baseline images from the DCE series [42,43]. The ROI-averaged and voxel (within the tumor ROI) DCE-MRI time-course data were separately fitted with different pharmacokinetic models: once with the one-compartment-two-parameter TM [36] and once with the two-compartment-three-parameter fast-exchange-regime (FXR)–allowed SSM [38]. Equations (1) and (2) represent the pharmacokinetic time-course expressions for the TM and FXR-SSM, respectively:

$$R_1(t) = r_1\left\{K^{trans}\int_0^t C_p(t')\exp(-K^{trans}/v_e(t-t'))dt'\right\} + R_{10}, \quad (1)$$

$$\begin{aligned} R_1(t) = (1/2)\Bigg[&\left\{2R_{1i} + r_1K^{trans}/v_e\int_0^t C_p(t')\exp(-K^{trans}/v_e(t-t'))dt' \right.\\ &\left. +(R_{10}-R_{1i}+1/\tau_i)/v_e\right\}\\ &-\left\{\left[2/\tau_i + (R_{1i}- R_{10}-1/\tau_i)/v_e - r_1K^{trans}/v_e\int_0^t C_p(t')\right.\right.\\ &\left.\left.\times\exp(-K^{trans}/v_e(t-t'))dt'\right]^2 + 4(1-v_e)/\tau_i^2v_e\right\}^{1/2}\Bigg], \end{aligned} \quad (2)$$

where $R_1(t)$ is the tissue longitudinal relaxation rate constant, $C_p(t')$ is the arterial plasma CA concentration time course, or arterial input function (AIF), R_{1i} is the intrinsic intracellular longitudinal relaxation rate constant, R_{10} (= $1/T_{10}$) is the pre-CA tissue R_1, r_1 is the tissue CA relaxivity, K^{trans} is the rate constant for CA plasma-to-interstitium transfer, v_e is the volume fraction of extravascular and extracellular

space, and τ_i is the mean intracellular water molecule lifetime. Both model fittings return K^{trans} and v_e parameter values, and the CA intravasation rate constant, k_{ep}, can be calculated as $k_{ep} = K^{trans}/v_e$. However, only the SSM fitting returns the τ_i parameter. Since the TM neglects the finite intercompartmental water exchange kinetics, assuming the water exchange MR system is always in the fast-exchange-limit condition, the linear relationship between $R_1(t)$ and tissue CA concentration, $C_t(t)$, shown in Equation (3) and implicit in Equation (1), is used:

$$R_1(t) = r_1 C_t(t) + R_{10}. \quad (3)$$

The SSM accounts for the finite water exchange kinetics during the CA passage through the tissue of interest, and consequently $R_1(t)$ is not linearly related to $C_t(t)$. The FXR-SSM takes into account transcytolemmal water exchange kinetics in the two-compartment model of intra- and extra-cellular compartments (in the extravascular space), but assumes single exponential longitudinal MR signal decay [38,39,41,44].

A population-averaged AIF was used for pharmacokinetic analysis of DCE-MRI data for each patient and each visit. This AIF was obtained by averaging individually measured AIFs from an axillary artery in a previous sagittal breast DCE-MRI study with higher temporal resolution [44], which employed the same CA injection protocol, including dose, injection rate, and injection vein (antecubital vein). Following the TM and SSM fittings of the DCE-MRI data, voxel-based parametric maps of the derived pharmacokinetic parameters were generated. The mean whole tumor pharmacokinetic parameter value estimated with each model at each visit was calculated as the average of single-slice ROI parameter values from the multiple image slices covering the whole tumor, weighted by the number of voxels in each ROI. For each imaging metric, including pharmacokinetic parameters and RECIST LD, the percent changes for later visits relative to V1, V21% (V2 relative to V1), V31%, and V41%, were calculated.

Pathological Analysis

The status of pathologic response (to NACT) for each breast tumor was determined by pathological analysis of the post-NACT resection specimen. The pathology parameters measured from the resection specimen under light microscopy include: cross sectional tumor size in two dimensions (d_1, d_2, measured [in mm] grossly and confirmed microscopically), estimated invasive tumor cellular density (f_{inv}), number of involved lymph nodes (LN), and the greatest tumor dimension (d_{met}) in the largest involved node. The Residual Cancer Burden (RCB) index value was calculated using Equation (4) published by Symmans et al [9]:

$$RCB = 1.4\left[f_{inv} * (d_1 d_2)^{1/2}\right]^{0.17} + \left[4\left(1-0.75^{LN}\right) d_{met}\right]^{0.17} \quad (4)$$

A complete pathologic response (pCR) is defined as the absence of residual invasive tumor (RCB = 0). A pathologic non-response (pNR) is defined as tumor cell density in resection specimen equal to or greater than that in core biopsy specimen. Pathologic partial response (pPR) is defined as findings intermediate between pCR and pNR. Non-pCR includes both pPR and pNR and can be further stratified into RCB classes based on RCB index values [9]: RCB-I: $0 < RCB \leq 1.36$; RCB-II: $1.36 < RCB \leq 3.28$; RCB-III: $RCB > 3.28$. Since the MRI metrics were measured from the primary breast tumor only, the in-breast component of RCB (the first term on the right hand side of Equation (4)) [23] was also computed for correlation with the MRI results. The same RCB index value ranges were used for defining in-breast RCB classes.

Statistical Analysis

Descriptive statistical analysis was conducted to summarize the pharmacokinetic parameter (returned by each model fitting) and RECIST LD values at each visit, as well as the percent changes of these imaging metrics relative to baseline (V1). In assessing the ability for early prediction of therapy response, the univariate logistic regression (ULR) analysis was used to correlate V1, V2, V3 MRI metrics, and the corresponding V21% and V31% changes, with dichotomous pathologic response endpoints, pCR *vs.* non-pCR. A ULR C statistics value, a measure equivalent to the area under the receiver operating characteristic curve, in the range of 0.9 to 1.0 indicates an excellent predictor; 0.8 to 0.9, a good predictor; 0.7 to 0.8, a fair predictor; <0.7, a poor predictor. A two-sample *t* test was used to evaluate the differences in imaging metrics and the corresponding percent changes between the pCR and non-pCR groups. In assessing the ability for evaluation of RCB (and in-breast RCB) following NACT completion, the ULR analysis was used to estimate the capabilities of V4 and V41% MRI metrics for discriminating RCB (and in-breast RCB) class, while the Spearman correlation (SC) analysis was used to correlate V4 and V41% MRI metrics with RCB (and in-breast RCB) index values.

Results

As shown in Table 1, pathological analyses of the surgical specimens revealed that 5 patients (5 primary tumors) achieved pCR following NACT, while the other 23 patients (24 primary tumors) all had pPR, or non-pCR. The RCB class for each tumor is also presented in Table 1.

Early Prediction of Pathologic Response

Table 2 lists the mean ± SD whole tumor MRI metric values of the pCR and non-pCR groups and the corresponding ULR C statistics values for early prediction of pCR *vs.* non-pCR. Only the absolute pharmacokinetic parameters and the V21% and V31% changes with $C \geq 0.8$, representing good to excellent early predictors, are listed. The C values for V21% and V31% RECIST LD changes are presented for

Table 2. Early Prediction of Pathologic Response (pCR *vs.* non-pCR)

MRI Metric	pCR	non-pCR		ULR C value
	Mean ± SD	Mean ± SD	*P* value	
V21% K^{trans}(TM)	−64% ± 9%	−14% ± 41%	.098	0.967
V21% k_{ep}(TM)	−77% ± 9%	−20% ± 44%	.050	0.957
V21% K^{trans}(SSM)	−71% ± 9%	−16% ± 50%	.052	0.957
V21% τ_i	41% ± 26%	−11% ± 25%	.018	0.946
V2 v_e(SSM)	0.78 ± 0.10	0.60 ± 0.14	.073	0.897
V21% v_e(TM)	80% ± 60%	35% ± 42%	.026	0.880
V21% v_e(SSM)	72% ± 41%	19% ± 28%	.033	0.880
V2 v_e(TM)	0.70 ± 0.37	0.29 ± 0.11	.018	0.864
V3 v_e(TM)	0.63 ± 0.31	0.32 ± 0.15	.035	0.845
V3 v_e(SSM)	0.81 ± 0.11	0.63 ± 0.15	.088	0.845
V1 τ_i (s)	0.53 ± 0.16	0.81 ± 0.26	.047	0.826
V31% v_e(SSM)	80% ± 54%	27% ± 30%	.041	0.810
V21% k_{ep}(SSM)	−77% ± 12%	−11% ± 94%	.092	0.804
V31% v_e(TM)	141% ± 115%	65% ± 85%	.070	0.804
V31% RECIST LD	−35% ± 21%	−26% ± 20%	.438	0.673
V21% RECIST LD	−15% ± 16%	−10% ± 11%	.320	0.609

ULR: univariate logistic regression; SD: standard deviation; *P* value: two-sample *t* test; TM: Tofts model; SSM: Shutter-Speed model.

comparison. The V21% changes in tumor K^{trans}(TM), K^{trans}(SSM), k_{ep}(TM), and τ_i provide excellent (C > 0.9) early discrimination of pCR and non-pCR, while V2 and V3 v_e estimated from either pharmacokinetic model, and their corresponding V21% and V31% changes, are good (0.8 < C < 0.9) markers for early prediction of response. The V21% and V31% changes in RECIST LD, however, are poor (C < 0.7) early predictors of response. Except for the RECIST LD changes, the differences in all other listed metrics between the two response groups are statistically significant ($P < .05$) or approaching significance. Other than τ_i at V1, which is a good early predictor of response with a C value of 0.826, no other pre-NACT MRI metrics have a C value greater than 0.7. Figure 1*A* shows the mean ± SD column graph of V21% changes in K^{trans}(TM), K^{trans}(SSM), k_{ep}(TM), v_e(TM), v_e(SSM), τ_i, and RECIST LD for the pCR and non-pCR groups. Note the substantially larger differences in the pharmacokinetic parameters between the two groups compared to RECIST LD. Figure 1*B* shows a similar graph for absolute TM and SSM v_e values of the two patient groups at V2 and V3.

To demonstrate differences in early changes of tumor pharmacokinetic parameters following NACT initiation, Figure 2 shows examples of K^{trans}(SSM), v_e(SSM), and τ_i maps at V1 and V2 for a pCR (Figure 2*A*, patient 12) and a non-pCR (Figure 2*B*, patient 3) patient. The color tumor parametric maps are in image slices approximately through the center of the tumor in every case, and the color scales are kept the same through the two visits for each tumor.

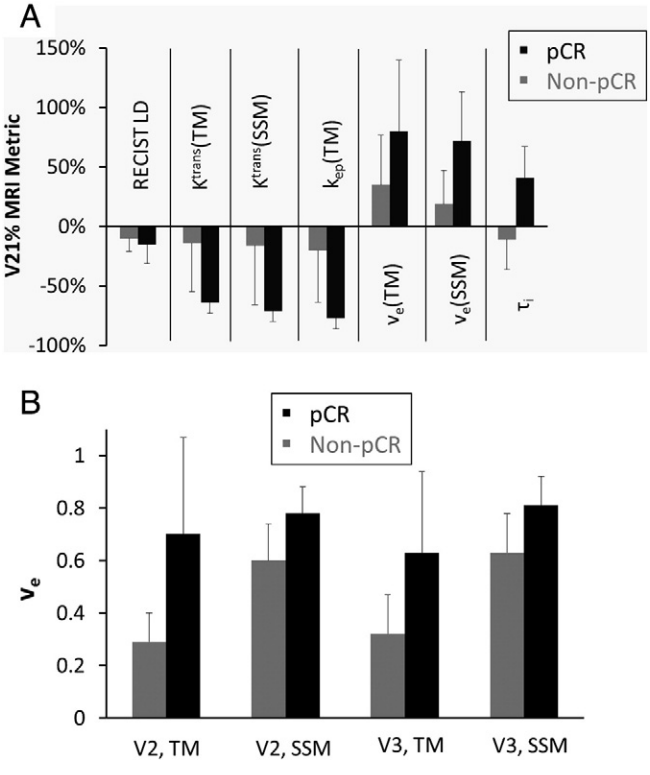

Figure 1. Column graphs of the (A) mean V21% change values of RECIST LD and several DCE-MRI metrics (K^{trans}, v_e, k_{ep}, and τ_i, estimated from the TM and SSM pharmacokinetic analyses) and (B) mean V2 and V3 v_e values (TM and SSM) for the pCR (black column) and non-pCR (gray column) patient groups. The error bar represents the standard deviation (SD). V21%: percent change of MRI metric at visit 2 (V2, after one NACT cycle) relative to visit 1 (V1, pre-NACT); V3: visit 3, midpoint of NACT.

There are no noticeable changes in the three parametric maps from V1 to V2 for the non-pCR, while the considerable decrease in K^{trans}(SSM) and increases in v_e(SSM) and τ_i are clearly visible for the pCR.

MRI evaluation of RCB after NACT

Table 3A presents the ULR C statistics values of several post-NACT MRI metrics for differentiating RCB and in-breast RCB classes of 0, I, II, and III. Only the metrics with C ≥ 0.7 (fair or better markers of RCB class) for in-breast RCB classes are listed, which include absolute values of V4 K^{trans}(SSM), K^{trans}(TM), k_{ep}(SSM), k_{ep}(TM), τ_i, and RECIST LD. The discriminative abilities of these metrics are improved slightly when in-breast RCB class is used in place of RCB class. There is not a single V41% change metric that is at least a fair marker of RCB or in-breast RCB class.

The SC coefficient, R, and the *P* value for statistical significance are summarized in Table 3B for correlation between RCB (and in-breast RCB) index value and post-NACT MRI metric value. Only those metrics with $P < 0.1$ are listed. As is the case of correlation with RCB class, the strength of SC is generally improved slightly when the in-breast RCB index value is used, and no V41% metric has a SC P value smaller than 0.1. The positive correlations between RCB and V4 RECIST LD, K^{trans}(SSM), and K^{trans}(TM) are statistically significant ($P < .05$) for both RCB and in-breast RCB values. The inverse correlation between RCB and V4 τ_i is significant ($P = .041$) for the in-breast RCB, while approaching significance ($P = .074$) for the RCB value. The positive correlation between RCB and V4 k_{ep}(SSM) is near statistical significance for both the RCB and in-breast RCB values. Figure 3 shows examples of linear regressions between the RCB (and in-breast RCB) index values and the V4 MRI metrics of RECIST LD (Figure 3*A*), K^{trans}(SSM) (Figure 3*B*), and τ_i (Figure 3*C*).

Discussion

Consistent with several previous studies [26–35] using DCE-MRI to assess breast cancer response to NACT, our initial findings from this study of a 28-patient cohort show that changes in tumor functions as measured by quantitative DCE-MRI are considerably more reliable early predictors of pCR compared to changes in imaging tumor size after only one of six or eight cycles of NACT. This suggests that therapy-induced tumor functional changes precede changes in tumor size. The percent changes of the K^{trans}, v_e, and k_{ep} parameters, as well as the SSM-unique τ_i parameter, are good to excellent early predictors of pathologic response. Additionally, the absolute values of v_e after one NACT cycle (V2) or at NACT midpoint (V3) are also good early predictors of response. Imaging tumor size measurement under the RECIST guidelines is the current standard of care for evaluation of tumor response to treatment. However, our results reveal that changes in RECIST LD after one NACT cycle, or even at midpoint of NACT (Table 2), are poor early predictors of response. For example, under the condition of 100% sensitivity for prediction of pCR (i.e., correctly classify all five pCRs in the study cohort), the specificities are 92% and 17% for V21% K^{trans}(TM) and V21% RECIST LD, respectively, meaning misclassification of only two out of 24 non-pCR tumors as pCRs when using V21% K^{trans}(TM) as the imaging metric *versus* 20 out of 24 non-pCRs as pCRs when using V21% RECIST LD as the imaging metric. The ability of minimally invasive imaging parameters, such as the DCE-MRI parameters, to accurately provide early prediction of therapy response may have profound importance in the emerging era of precision and personalized medicine. Early identification of non-responders to a

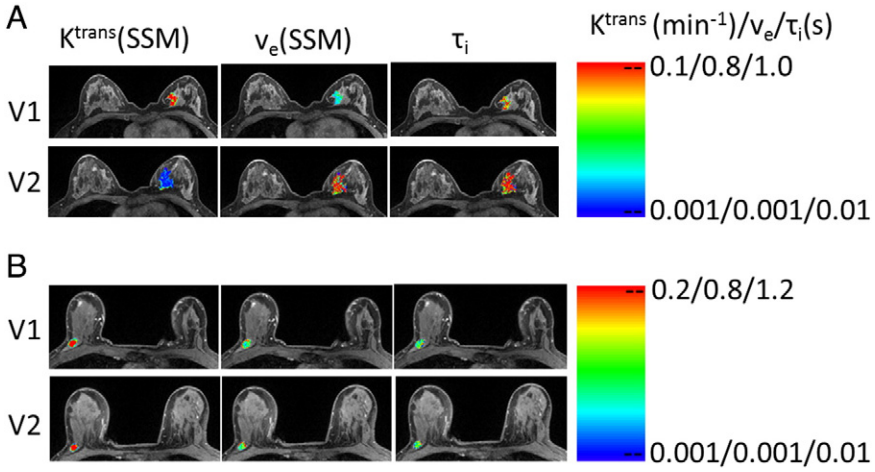

Figure 2. V1 (pre-NACT) and V2 (after one NACT cycle) color parametric maps of K^{trans}(SSM), v_e(SSM), and τ_i from a pCR (A, left breast, patient 12) and a non-pCR (B, right breast, patient 3) breast tumor. The maps were generated for tumor ROIs defined on multiple image slices, and the ones on the image slice through the central portion of the tumor are displayed here. For each tumor, the color scale of each DCE-MRI metric is kept the same between the two visits for easy visualization of NACT-induced changes.

therapy regimen may allow rapid decision making in adjusting the treatment plan, e.g., changing drugs and/or undergoing surgery early, to spare these patients from the morbidity caused by ineffective and toxic chemotherapy agents. This will have significant positive impact on healthcare cost savings and patient wellbeing. Using this cohort as an example, if V21% K^{trans}(TM) had been used as the imaging marker for early prediction of therapy response in clinical care, 22 out of 24 non-pCRs would have been correctly classified after only one NACT cycle and could have been treated with different therapy regimens or stratified for novel therapy trials.

Accurate imaging assessment of RCB after NACT can lead to better staging for surgery and more informed decision making in breast conservation surgery *versus* mastectomy. Though RECIST LD is not a good early predictor of pathologic response, its value measured after NACT completion (V4) is indicative of the RCB class and index value (Tables 3A and 3B; Figure 3*A*). The post-NACT DCE-MRI parameters that are fair to good markers of RCB class and correlate significantly with RCB index value include K^{trans} (estimated from either of the two models) and τ_i. Unsurprisingly, since the MRI metrics were measured from the primary tumor only, the correlations with RCB are slightly improved when the in-breast RCB class and value are used (Tables 3A and 3B; Figure 3). With a larger patient cohort, meaningful multivariate analysis may be performed to potentially identify a combination of imaging metrics including both tumor size and DCE-MRI functional parameters that can provide even more accurate measure of RCB.

Since cytotoxic drugs such as doxorubicin, cyclophosphamide, and paclitaxel were used throughout the NACT regimen for each patient studied, it is to be expected that increases in v_e after one NACT cycle or at NACT midpoint are found to be good early predictors of response. The therapy-induced cancer cell death presumably leads to decrease in the extravascular, intracellular volume fraction, v_i ($\equiv 1 - v_e$), which is dominated by decrease in cell density [41], and hence increase in v_e. However, at the early stage of NACT a decrease in v_i is not necessarily associated with a decrease in perfused tumor area, or contrast-enhanced MRI tumor size, the basis for RECIST LD measurement. This hypothesis on why the v_e percent change is a good early predictor of response while the RECIST LD percent change is a poor predictor needs to be further tested in future studies. On the other hand, the post-NACT (V4) RECIST LD is a better measure of RCB than v_e. This could be due to the fact that the RCB calculation (Equation (4)) includes dominant contribution from the product of cross sectional tumor sizes d_1 and d_2 measured from the resection specimen, while the association of v_i (or $1 - v_e$) with f_{inv} is not as distinct - the former measures overall cell density [41] while the latter characterizes invasive cancer cell density.

The percent deceases in K^{trans} and k_{ep} after one NACT cycle are good to excellent early predictors of response, suggesting these

Table 3A. Discrimination of Post-NACT RCB Class

MRI Metric	ULR C value	
	RCB class	In-breast RCB class
V4 K^{trans}(SSM)	0.801 (0.680, 0.922)	0.837 (0.734, 0.940)
V4 K^{trans}(TM)	0.797 (0.669, 0.925)	0.833 (0.708, 0.958)
V4 τ_i	0.783 (0.647, 0.919)	0.792 (0.634, 0.950)
V4 RECIST LD	0.727 (0.586, 0.868)	0.732 (0.538, 0.870)
V4 k_{ep}(SSM)	0.697 (0.540, 0.854)	0.719 (0.520, 0.890)
V4 k_{ep}(TM)	0.694 (0.553, 0.835)	0.705 (0.527, 0.857)

Imaging results are missing from a pCR patient (patient 20), who declined the V4 MRI study due to personal reasons. The values in the parentheses are 95% confidence intervals (CIs).

Table 3B. Spearman Correlation of Post-NACT RCB Index Value with MRI Metric Value

MRI Metric	RCB		In-breast RCB	
	R	*P*	R	*P*
V4 RECIST LD	0.532	.009	0.485	.019
V4 K^{trans}(SSM)	0.463	.022	0.643	.001
V4 K^{trans}(SM)	0.463	.022	0.618	.002
V4 τ_i	−0.380	.074	−0.429	.041
V4 k_{ep}(SSM)	0.366	.078	0.376	.070

R: Spearman correlation coefficient; $P < 0.05$ indicates statistically significant correlation.
Imaging results are missing from a pCR patient (patient 20), who declined the V4 MRI study due to personal reasons.

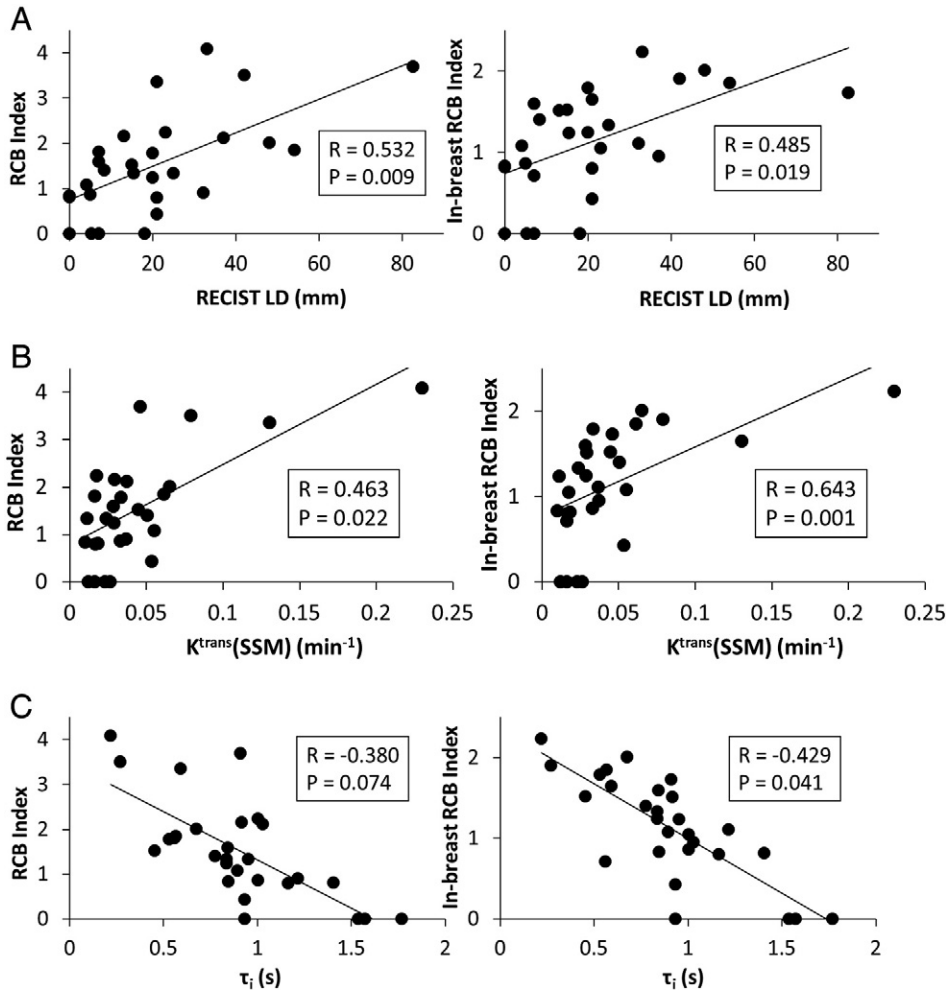

Figure 3. Scatter plots of pathologically measured RCB and in-breast RCB index values (from post-NACT resection specimens) against post-NACT (V4) MRI metrics: (A) RECIST LD, (B) K^{trans}(SSM), and (C) τ_i. The straight line in each panel represents a linear regression. The Spearman correlation coefficient R and P values for the three imaging metrics are listed in Table 3B and shown in each panel. Note the inverse relationship between RCB (and in-breast RCB) and τ_i. Imaging results are missing from a pCR patient (patient 20), who declined the V4 MRI study due to personal reasons.

imaging metrics of perfusion and permeability may be sensitive parameters for prediction of NACT response. The therapy-induced changes in these microvascular properties are probably due to NACT secondary effects [14], since none of the standard of care or experimental drugs used in this cohort is known to be antiangiogenic. It has been suggested [45] that cytotoxic chemotherapy agents may affect tumor vasculature by interfering with endothelial cell function without causing endothelial cell death or interfering with a specific portion of the angiogenic cascade. The results from this study and others [26–34] indicate that it is the early changes in K^{trans} and k_{ep}, not the perfused tumor area as measured by RECIST LD, that are good predictors of therapy response. This observation supports the hypothesis that the chemotherapeutics effects tumor vasculature without causing endothelial cell death [45]. One interesting finding is that though the V31% change in v_e is still a good early predictor of response (Table 2), the V31% changes in K^{trans} and k_{ep} are degraded to only fair predictors of response (not shown). For example, V31% K^{trans}(TM) and V31% K^{trans}(SSM) have ULR C values of 0.756 and 0.750, respectively. The decrease in the predictive ability is because the pCRs have such larger decreases in K^{trans} and k_{ep} at V2 compared to non-pCRs that, by V3 (NACT midpoint), the percent changes (relative to baseline, V31%) in these metrics of the non-pCRs, though still smaller, draw near to those of the pCRs. Therefore, it is important to detect early microvascular changes with DCE-MRI, as they are better indicators of complete response to NACT than later changes.

The τ_i parameter is used to account for the effects of transcytolemmal water exchange kinetics and unique to the SSM method. A recent NMR spectroscopy study of yeast cell suspension [40] shows that the reciprocal of τ_i, k_{io} ($\equiv 1/\tau_i$), the first-order rate constant for equilibrium cellular water efflux, is positively associated with cellular ATP levels. The *in vivo* association of cellular ATP decrease with k_{io} decrease was demonstrated by a DCE-MRI and ^{31}P MR spectroscopy study of a murine melanoma model treated with lonidamine [46]. A series of enzymatic and genetic manipulations on cell suspensions, perfused tissue, *in vivo* animal models, and human data have shown that k_{io} measures the homeostatic turnover of the cell membrane Na^+,K^+-ATPase [NKA] [41]. Previously, it has not been possible to measure homeostatic NKA activity *in vivo*. In this study the V21% change in breast tumor τ_i is an excellent early predictor of pathologic response (Table 2). The pCRs show significant increase in

τ_i (or decrease in k_{io}) compared to non-pCRs after one NACT cycle, consistent with a substantial decrease in tumor metabolic activities early after NACT initiation being generally a good indicator of complete response. It is interesting to note that the pCR group has smaller pre-NACT (V1) τ_i values and thus greater metabolic turnover than the non-pCR group (Table 2), and V1 τ_i is the best predictor of response (a good metric with ULR C = 0.826) of all the V1 MRI metrics. The post-NACT (V4) τ_i is well correlated with the RCB index value in an inverse relationship (Table 3B and Figure 3*C*). These findings suggest that, over the course of the entire NACT regimen, the good responders have greater increases in τ_i, or decreases in metabolic activity, than the poor responders. In fact, from V1 to V4 the mean τ_i value of the pCR group is increased from 0.53 to 1.45 s, while that of the non-pCR group remains stable (0.81 to 0.82 s). The importance of τ_i as an imaging parameter for evaluation of breast cancer response to NACT is further confirmed by a pre-clinical DCE-MRI study of a genetically engineered mouse model of human breast tumor [47], which shows τ_i increase with almost no v_i change following treatment with an experimental targeted, non-cytotoxic drug.

The DCE-MRI data acquired in this study were analyzed with both the TM and SSM. For the three parameters that can be estimated with both models, K^{trans}, v_e, and k_{ep}, the percent changes of these parameters in the early stage of NACT and the absolute values after NACT have similar capabilities for early prediction of response and evaluation of RCB, respectively, when comparing the two models. This is likely due to the fact that the underestimation of the K^{trans} and v_e parameters in malignant tumors by the TM relative to the SSM is generally systematic [27,44]. The systematic parameter variations between the two models were largely cancelled in percent change calculation, or caused parameter values of each tumor to shift in the same direction when estimated from one pharmacokinetic model or the other. As a result, TM and SSM analyses performed equally well in early prediction and evaluation of therapy response. Li et al. [28] reported similar findings for early prediction of breast cancer response to NACT. Nonetheless, water exchange across tissue compartments is a real physiological phenomenon. Therefore, the SSM analysis approach should be used when T_1-weighted DCE-MRI data are acquired with a protocol that is sensitive to water exchange, which usually also results in better signal-to-noise ratio [48]. Furthermore, the SSM analysis allows estimation of the metabolic activity imaging metric k_{io}, adding a metabolic dimension to DCE-MRI, which is conventionally considered only as a functional imaging method for assessment of tissue microvasculature. As discussed above, the τ_i (or k_{io}^{-1}) parameter is a very good marker for early prediction of response and accurate assessment of residual disease. The ability to characterize synergistic microvascular properties and cellular energetic metabolism simultaneously may harbor great promise for SSM DCE-MRI as an imaging tool to study the tumor microenvironment, and its response to treatment.

This study has several major limitations. First, with only 29 primary breast tumors, the sample size of the study cohort is small. The discriminative ability of a metric tends to be overestimated when the sample size is small. This is possibly the reason why the ULR C values of several DCE-MRI metrics obtained in this study for early prediction of breast cancer response to NACT are greater than the equivalent area under the receiver operating characteristic curve values reported by similar studies with larger cohort sizes [22,23,26,28,29]. Thus, it is important to validate the initial findings from this cohort with a larger patient population, especially for new findings specific to this study such as changes in v_e and τ_i as early predictors of response. Second, as a result of small sample size, the imaging results are not stratified by receptor status-based breast cancer molecular subtypes in correlation with pathology endpoints. The number of patients is simply not adequate to draw meaningful conclusions in early discrimination of pCR and non-pCR or evaluation of RCB for each breast tumor subtype, and make comparisons between the subtypes. As such, the initial findings reported here reflect the average results from a general breast cancer population undergoing NACT. With continuing subject accrual, we will be able to examine and compare the utility of DCE-MRI for evaluation of therapy response in each breast cancer subtype in the future. Additionally, the small sample size also precludes meaningful multivariate analysis of the MRI metrics for further improvement in assessing therapy response. Third, mean tumor MRI metric values were used in this study for correlation with the pathology endpoints. It is well known that malignant tumors are heterogeneous in nature [41] and responses to treatment are likely heterogeneous as well. However, the heterogeneity in breast tumor functional changes in response to NACT was not captured in computing mean DCE-MRI parameter values. Recent studies show that texture analysis of tumor heterogeneity manifest in either raw image data [49–51] or parametric maps of kinetic features [52,53] can be a valuable tool for evaluation of breast cancer therapy response. With voxel-based parametric maps of DCE-MRI metrics already generated in this study, texture analysis of these maps could potentially be performed. Measurement and integration of changes in both mean values and texture features of DCE-MRI metrics may further improve the robustness of quantitative DCE-MRI for assessment of therapy response.

In conclusion, in this DCE-MRI study of 29 primary breast tumors undergoing NACT, we have shown that changes in quantitative functional MRI metrics estimated by either TM or SSM analysis of DCE-MRI data provide substantially better early prediction of pathologic response to NACT than changes in imaging tumor size as measured by RECIST LD. Along with post-NACT RECIST LD, several post-NACT DCE-MRI parameters are good markers of RCB. The TM and SSM analyses perform equally well for early prediction of response and evaluation of RCB. However, the SSM method provides additional assessment of tumor metabolic activity changes in response to NACT, and the SSM-unique τ_i parameter is the only pre-therapy MRI metric that provides good early prediction of response. Future translation of quantitative DCE-MRI into clinical practice may help facilitate personalized treatment regimens for individual breast cancer patients and more informed decision making in breast conservation surgery *vs.* mastectomy.

Acknowledgements

The authors thank the breast cancer patients who voluntarily participated in this research study and Mr. William Woodward for assistance in breast DCE-MRI data acquisition.

References

[1] Hayes DF and Schott AF (2015). Neoadjuvant chemotherapy: what are the benefits for the patient and for the investigator? *J Natl Cancer Inst Monogr* **2015**, 36–39.

[2] Schott AF and Hayes DF (2012). Defining the benefits of neoadjuvant chemotherapy for breast cancer. *J Clin Oncol* **30**, 1747–1749.

[3] Fisher B, Bryant J, Wolmark N, Mamounas E, Brown A, and Fisher ER, et al (1998). Effect of preoperative chemotherapy on the outcome of women with operable breast cancer. *J Clin Oncol* **16**, 2672–2685.

[4] Mauri D, Pavlidis N, and Ioannidis JP (2005). Neoadjuvant versus adjuvant systemic treatment in breast cancer: a meta-analysis. *J Natl Cancer Inst* **97**, 188–194.

[5] Redden MH and Fuhrman GM (2013). Neoadjuvant chemotherapy in the treatment of breast cancer. *Surg Clin North Am* **93**, 493–499.

[6] Bonnefoi H, Litiere S, Piccart M, MacGrogan G, Fumoleau P, Brain E, Petit T, Rouanet P, Jassem J, and Moldovan C, et al (2014). Pathological complete response after neoadjuvant chemotherapy is an independent predictive factor irrespective of simplified breast cancer intrinsic subtypes: a landmark and two-step approach analyses from the EORTC 10994/BIG 1-00 phase III trial. *Ann Oncol* **25**, 1128–1136.

[7] von Minckwitz G, Untch M, Blohmer JU, Costa SD, Eidtmann H, Fasching PA, Gerber B, Eiermann W, Hilfrich J, and Huober J, et al (2012). Definition and impact of pathologic complete response on prognosis after neoadjuvant chemotherapy in various intrinsic breast cancer subtypes. *J Clin Oncol* **30**, 1796–1804.

[8] Kong X, Moran MS, Zhang N, Haffty B, and Yang Q (2011). Meta-analysis confirms achieving pathological complete response after neoadjuvant chemotherapy predicts favorable prognosis for breast cancer patients. *Eur J Cancer* **47**, 2084–2090.

[9] Symmans WF, Peintinger F, Hatzis C, Rajan R, Kuerer H, Valero V, Assad L, Poniecka A, Hennessy B, and Green M, et al (2007). Measurement of residual breast cancer burden to predict survival after neoadjuvant chemotherapy. *J Clin Oncol* **25**, 4414–4422.

[10] Gonzalez-Angulo AM, Morales-Vasquez F, and Hortobagyi GN (2007). Overview of resistance to systemic therapy in patients with breast cancer. *Adv Exp Med Biol* **608**, 1–22.

[11] Zambetti M, Mansutti M, Gomez P, Lluch A, Dittrich C, Zamagni C, Ciruelos E, Pavesi L, Semiglazov V, and De Benedictis E, et al (2012). Pathological complete response rates following different neoadjuvant chemotherapy regimens for operable breast cancer according to ER status, in two parallel, randomized phase II trials with an adaptive study design (ECTO II). *Breast Cancer Res Treat* **132**, 843–851.

[12] Therasse P, Arbuck SG, Eisenhauer EA, Wanders J, Kaplan RS, Rubinstein L, Verweij J, Van Glabbeke M, van Oosterom AT, and Christian MC, et al (2000). New guidelines to evaluate the response to treatment in solid tumors. European Organization for Research and Treatment of Cancer, National Cancer Institute of the United States, Nation Cancer Institute of Canada. *J Natl Cancer Inst* **92**, 205–216.

[13] O'Connor JPB, Jackson A, Parker GJM, Roberts C, and Jayson GC (2012). Dynamic contrast-enhanced MRI in clinical trials of antivascular therapies. *Nat Rev Clin Oncol* **9**, 167–177.

[14] Leach MO, Morgan B, Tofts PS, Buckley DL, Huang W, Horsfield MA, Chenevert TL, Collins DJ, Jackson A, and Lomas D, et al (2012). Imaging vascular function for early stage clinical trials using dynamic contrast-enhanced magnetic resonance imaging. *Eur Radiol* **22**, 1451–1464.

[15] Padhani AR and Miles KA (2010). Multiparametric imaging of tumor response to therapy. *Radiology* **256**, 348–364.

[16] Harry VN, Semple SI, Parkin DE, and Gilbert FJ (2010). Use of new imaging techniques to predict tumor response to therapy. *Lancet Oncol* **11**, 92–102.

[17] Lobbes MBI, Prevos R, Smidt M, Tjan-Heijnen VCG, van Goethem M, Schipper R, Beets-Tan RG, and Wildberger JE (2013). The role of magnetic resonance imaging in assessing residual disease and pathologic complete response in breast cancer patients receiving neoadjuvant chemotherapy: a systematic review. *Insights Imaging* **4**, 163–175.

[18] Marinovich ML, Sardanelli F, Ciatto S, Mamounas E, Brennan M, Macaskill P, Irwig L, von Minckwitz G, and Houssami N (2012). Early prediction of pathologic response to neoadjuvant chemotherapy in breast cancer: systematic review of the accuracy of MRI. *Breast* **21**, 669–677.

[19] Wu LM, Hu JN, Gu HY, Hua J, Chen J, and Xu JR (2012). Can diffusion-weighted MR imaging and contrast-enhanced MR imaging precisely evaluate and predict pathological response to neoadjuvant chemotherapy in patients with breast cancer? *Breast Cancer Res Treat* **135**, 17–28.

[20] Pickles MD, Lowry M, Manton DJ, and Turnbull LW (2015). Prognostic value of DCE-MRI in breast cancer patients undergoing neoadjuvant chemotherapy: a comparison with traditional survival indicators. *Eur Radiol* **25**, 1097–1106.

[21] Woolf DK, Padhani AR, Taylor NJ, Gogbashian A, Li SP, Beresford MJ, Ah-See ML, Stirling J, Collins DJ, and Makris A (2014). Assessing response in breast cancer with dynamic contrast-enhanced magnetic resonance imaging: are signal intensity-time curves adequate? *Breast Cancer Res Treat* **147**, 335–343.

[22] Abramson RG, Li X, Hoyt TL, Su PF, Arlinghaus LR, Wilson KJ, Abramson VG, Chakravarthy AB, and Yankeelov TE (2013). Early assessment of breast cancer response to neoadjuvant chemotherapy by semi-quantitative analysis of high-temporal resolution DCE-MRI: preliminary results. *Magn Reson Imaging* **31**, 1457–1464.

[23] Hylton NM, Blume JD, Bernreuter WK, Pisano ED, Rosen MA, Morris EA, Weatherall PT, Lehman CD, Newstead GM, and Polin S, et al (2012). Locally advanced breast cancer: MR imaging for prediction of response to neoadjuvant chemotherapy – results from ACRIN 6657/I-SPY trial. *Radiology* **263**, 663–672.

[24] Johansen R, Jensen LR, Rydland J, Goa PE, Kvistad KA, Bathen TF, Axelson DE, Lundgren S, and Gribbestad IS (2009). Predicting survival and early clinical response to primary chemotherapy for patients with locally advanced breast cancer using DCE-MRI. *J Magn Reson Imaging* **29**, 1300–1307.

[25] Martincich L, Montemurro F, De Rosa G, Marra V, Ponzone R, Cirillo S, Gatti M, Biglia N, Sarotto I, and Sismondi P, et al (2004). Monitoring response to primary chemotherapy in breast cancer using dynamic contrast-enhanced magnetic resonance imaging. *Breast Cancer Res Treat* **83**, 67–76.

[26] Li X, Kang H, Arlinghaus LR, Abramson RG, Chakravarthy AB, Abramson VG, Farley J, Sanders M, and Yankeelov TE (2014). Analyzing spatial heterogeneity in DCE- and DW-MRI parametric maps to optimize prediction of pathologic response to neoadjuvant chemotherapy in breast cancer. *Transl Oncol* **7**, 14–22.

[27] Huang W, Li X, Chen Y, Li X, Chang MC, Oborski MJ, Malyarenko DI, Muzi M, Jajamovich GH, and Fedorov A, et al (2014). Variations of dynamic contrast-enhanced magnetic resonance imaging in evaluation of breast cancer therapy response: a multicenter data analysis challenge. *Transl Oncol* **7**, 153–166.

[28] Li X, Arlinghaus LR, Ayers GD, Chakravarthy AB, Abramson RG, Abramson VG, Atuegwu N, Farley J, Mayer IA, and Kelley MC, et al (2014). DCE-MRI analysis methods for predicting the response of breast cancer to neoadjuvant chemotherapy: pilot study findings. *Magn Reson Med* **71**, 1592–1602.

[29] Tateishi U, Miyake M, Nagaoka T, Terauchi T, Kubota K, Kinoshita T, Daisaki H, and Macapinlac HA (2012). Neoadjuvant chemotherapy in breast cancer: prediction of pathologic response with PET/CT and dynamic contrast-enhanced MR imaging—prospective assessment. *Radiology* **263**, 53–63.

[30] Li SP, Makris A, Beresford MJ, Taylor NJ, Ah-See MLW, Stirling JJ, d'Arcy JA, Collins DJ, Kozarski R, and Padhani AR (2011). Use of dynamic contrast-enhanced MR imaging to predict survival in patients with primary breast cancer undergoing neoadjuvant chemotherapy. *Radiology* **260**, 68–78.

[31] Jensen LR, Garzon B, Heldahl MG, Bathen TF, Lundgren S, and Gribbestad IS (2011). Diffusion-weighted and dynamic contrast-enhanced MRI in evaluation of early treatment effects during neoadjuvant chemotherapy in breast cancer patients. *J Magn Reson Imaging* **34**, 1099–1109.

[32] Ah-See MLW, Makris A, Taylor NJ, Harrison M, Richman PI, Burcombe RJ, Stirling JJ, d'Arcy JA, Collins DJ, and Pittam MR, et al (2008). Early changes in functional dynamic magnetic resonance imaging predict for pathologic response to neoadjuvant chemotherapy in primary breast cancer. *Clin Cancer Res* **14**, 6580–6589.

[33] Yankeelov TE, Lepage M, Chakravarthy A, Broome EE, Niermann KJ, Kelley MC, Meszoely I, Mayer IA, Herman CR, and McManus K, et al (2007). Integration of quantitative DCE-MRI and ADC mapping to monitor treatment response in human breast cancer: initial results. *Magn Reson Imaging* **25**, 1–13.

[34] Padhani AR, Hayes C, Assersohn L, Powles T, Makris A, Suckling J, Leach MO, and Husband JE (2006). Prediction of clinicopathologic response of breast cancer to primary chemotherapy at contrast-enhanced MR imaging: initial clinical results. *Radiology* **239**, 361–374.

[35] Pickles MD, Lowry M, Menton DJ, Gibbs P, and Turnbull LW (2005). Role of dynamic contrast enhanced MRI in monitoring early response of locally advanced breast cancer to neoadjuvant chemotherapy. *Breast Cancer Res Treat* **91**, 1–10.

[36] Tofts PS and Kermode AG (1991). Measurement of the blood-brain barrier permeability and leakage space using dynamic MR imaging. *Magn Reson Med* **17**, 357–367.

[37] Tofts PS, Brix G, Buckley DL, Evelhoch JL, Henderson E, Knopp MV, Larsson HB, Lee TY, Mayr NA, and Parker GJ, et al (1999). Estimating kinetic parameters from dynamic contrast-enhanced T1-weighted MRI of a diffusable tracer: standardized quantities and symbols. *J Magn Reson Imaging* **10**, 223–232.

[38] Yankeelov TE, Rooney WD, Li X, and Springer CS (2003). Variation of the relaxographic "Shutter-Speed" for transcytolemmal water exchange affects the CR bolus-tracking curve shape. *Magn Reson Med* **50**, 1151–1169.

[39] Li X, Rooney WD, and Springer CS (2005). A unified pharmacokinetic theory for intravascular and extracellular contrast agents. *Magn Reson Med* **54**, 1351–1359 [Erratum. Magn Reson Med 2006;55:1217.].

[40] Zhang Y, Poirier-Quinot M, Springer CS, and Balschi JA (2011). Active trans-plasma membrane water cycling in yeast is revealed by NMR. *Biophys J* **101**, 2833–2842.

[41] Springer CS, Li X, Tudorica LA, Oh KY, Roy N, Chui SYC, Naik AM, Holtorf ML, Afzal A, and Rooney WD, et al (2014). Intratumor mapping of intracellular water lifetime: metabolic images of breast cancer? *NMR Biomed* **27**, 760–773.

[42] Tudorica LA, Oh KY, Roy N, Kettler MD, Chen Y, Hemmingson SL, Afzal A, Grinstead JW, Laub G, and Li X, et al (2012). A feasible high spatiotemporal resolution breast DCE-MRI protocol for clinical settings. *Magn Reson Imaging* **30**, 1257–1267.

[43] Huang W, Wang Y, Panicek DM, Schwartz LH, and Koutcher JA (2009). Feasibility of using limited-population-based average R_{10} for pharmacokinetic modeling of osteosarcoma dynamic contrast-enhanced MRI data. *Magn Reson Imaging* **27**, 852–858.

[44] Huang W, Tudorica LA, Li X, Thakur SB, Chen Y, Morris EA, Tagge IJ, Korenblit M, Rooney WD, and Koutcher JA, et al (2011). Discrimination of benign and malignant breast lesions by using shutter-speed dynamic contrast-enhanced MR imaging. *Radiology* **261**, 394–403.

[45] Miller KD, Sweeney CJ, and Sledge GW (2001). Redefining the target: chemotherapeutics as antiangiogenics. *J Clin Oncol* **19**, 1195–1206.

[46] Nath K, Paudyal R, Nelson DS, Pickup S, Zhou R, Leeper DB, Heitjan DF, Springer CS, Poptani H, and Glickson JD (2014). Acute changes in cellular-interstitial water exchange rate in DB-1 melanoma xenografts after lonidamine administration as a marker of tumor energetics and ion transport. *Proc Intl Soc Magn Reson Med* **22**, 2757.

[47] Springer CS, Li X, Jayatilake ML, Pike MM, Rooney WD, Sears RC, and Huang W (2015). Metabolic imaging of early tumor therapy. *Proc Intl Soc Magn Reson Med* **23**, 3860.

[48] Li X, Huang W, and Rooney WD (2012). Signal-to-noise ratio, contrast-to-noise ratio, and pharmacokinetic modeling considerations in dynamic-contrast-enhanced magnetic resonance imaging. *Magn Reson Imaging* **30**, 1313–1322.

[49] Ahmed A, Gibbs P, Pickles M, and Turbull L (2013). Texture analysis in assessment and prediction of chemotherapy response in breast cancer. *J Magn Reson Imaging* **38**, 89–101.

[50] Teruel JR, Heldahl MG, Goa PE, Pickles M, Lundgren S, Bathen TF, and Gibbs P (2014). Dynamic contrast-enhanced MRI texture analysis for pretreatment prediction of clinical and pathological response to neoadjuvant chemotherapy in patients with locally advanced breast cancer. *NMR Biomed* **27**, 887–896.

[51] Parikh J, Selmi M, Charles-Edwards G, Glendenning J, Ganeshan B, Verma H, Mansi J, Harries M, Tutt A, and Goh V (2014). Changes in primary breast cancer heterogeneity may augment midtreatment MR imaging assessment of response to neoadjuvant chemotherapy. *Radiology* **272**, 100–112.

[52] Golden DI, Lipson JA, Telli ML, Ford JM, and Rubin DL (2013). Dynamic contrast-enhanced MRI-based biomarkers of therapeutic response in triple-negative breast cancer. *J Am Med Inform Assoc* **20**, 1059–1066.

[53] Ashraf A, Gaonkar B, Mies C, DeMichele A, Rosen M, Davatzikos C, and Kontos D (2015). Breast DCE-MRI kinetic heterogeneity tumor markers: preliminary associations with neoadjuvant chemotherapy response. *Transl Oncol* **8**, 154–162.